

## Epitaxial Retrieval of a Disappearing Polymorph

Published as part of the *Crystal Growth & Design* virtual special issue IYCr 2014 - Celebrating the International Year of Crystallography

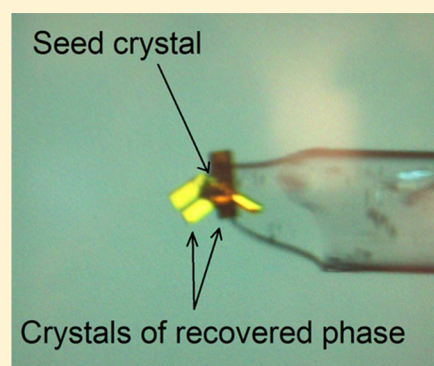
Jeremiah P. Tidey,<sup>†</sup> Alice E. O'Connor,<sup>†</sup> Alexander Markevich,<sup>†</sup> Elena Bichoutskaia,<sup>†</sup> Joseph J. P. Cavan,<sup>†</sup> Geoffrey A. Lawrance,<sup>‡</sup> Henry L. S. Wong,<sup>†</sup> Jonathan McMaster,<sup>†</sup> Martin Schröder,<sup>\*,†</sup> and Alexander J. Blake<sup>\*,†</sup>

<sup>†</sup>School of Chemistry, University of Nottingham, University Park, Nottingham, Nottinghamshire, United Kingdom NG7 2RD

<sup>‡</sup>Discipline of Chemistry, School of Environmental and Life Sciences, The University of Newcastle, Callaghan, NSW 2308, Australia

### Supporting Information

**ABSTRACT:** Recrystallization of  $[\text{PdCl}_2([\text{9}] \text{aneS}_2\text{O})]$  ( $[\text{9}] \text{aneS}_2\text{O}$  = 1-oxa-4,7-dithiacyclononane), **1**, and  $[\text{PtCl}_2([\text{9}] \text{aneS}_2\text{O})]$ , **2**, by diffusion of  $\text{Et}_2\text{O}$  vapor into solutions of the complexes in  $\text{MeNO}_2$  yielded three phases of **1** and two phases of **2**. The known phase of **1**, herein designated  $\alpha$ -**1**, was obtained under ambient conditions. A second phase, designated  $\beta$ -**1**, was initially also obtained by this method; however, following the advent of a third phase,  $\gamma$ -**1**, all subsequent efforts over a period of a year to crystallize  $\beta$ -**1** yielded either  $\gamma$ -**1**, obtained by carrying out the recrystallization at elevated temperature, or  $\alpha$ -**1**, commonly found throughout the study. This persistent absence of a phase which could initially be crystallized with ease led us to the conclusion that  $\beta$ -**1** was an example of a “disappearing polymorph”. The first phase obtained of **2**, designated  $\alpha$ -**2**, was obtained by recrystallization under ambient conditions and is isomorphous and isostructural with  $\alpha$ -**1**. The second phase  $\beta$ -**2** was obtained by slight elevation of the recrystallization temperature and was found to be isomorphous and isostructural with  $\beta$ -**1**. Subsequently,  $\beta$ -**2** was used to seed the growth of the disappearing polymorph  $\beta$ -**1**. No third phase of **2** ( $\gamma$ -**2**) has been isolated thus far.



### INTRODUCTION

Polymorphism, the phenomenon of a material packing in multiple distinct crystalline forms, is a well-known occurrence in the field of crystallography. In the case of organic compounds this is particularly well documented: for example, an analysis of 245 polymorph screens carried out at the SSCI (Solid State Chemical Information, West Lafayette) showed that ca. 50% of the compounds studied exhibited polymorphism.<sup>1</sup> However, it should be noted that this work was specifically a search for polymorphism and, although showing that it is a widespread phenomenon, the study does not correspond with the overall statistics from the Cambridge Structural Database (CSD). In their recent review,<sup>2</sup> Cruz-Cabeza and Bernstein present an analysis of conformational polymorphism in organic compounds using the “best R factor” subset of the CSD (Nov. 2011 release)<sup>3</sup> and found that, of the 351 979 structures in the subset, 2770 corresponded to 1297 truly polymorphic organic molecules. It was also found that increases in the size and conformational flexibility of molecules do not appear to be directly related to whether or not a compound exhibited polymorphism. Their findings show that polymorphism arises from the presence of multiple competing intermolecular interactions combined with the possible conformations the molecule can adopt: these factors can give

rise to a variety of packing systems that may differ only slightly in energy. Fewer polymorphic systems are reported for coordination complexes:<sup>4,5</sup> a comparative survey of the CSD (Nov. 2013 release plus three updates; “best R factor” subset used) found the ratio of organic to organometallic compounds exhibiting polymorphism to be ca. 3:2. One likely reason for this is simply that the phenomenon is not routinely investigated in these complexes: to quote McCrone, “the number of polymorphic forms for a given compound is proportional to the time and money spent in research on that compound”.<sup>6</sup> Polymorphism is of paramount importance in the pharmaceutical industry where different phases can have vastly different physical properties<sup>7</sup> and so the compounds produced, typically organic in nature, are intensely screened to understand their habits, properties, and preferences. Coordination complexes are often synthesized in a research environment where the aim of the crystallographic study is to characterize the molecular structure: usually there is neither need nor incentive to screen for polymorphs.

Received: July 1, 2014

Revised: December 2, 2014

Published: December 3, 2014

A great number of techniques exist to aid the search for different crystal forms, including variation of the solvent system and the use of additives.<sup>8</sup> Nevertheless, it is not unknown for a phase to be obtained and later “disappear” following the appearance of a more thermodynamically stable form: seeds of this new form pervade the crystallization environment and prevent the formation of the previously obtained less stable polymorph: this phenomenon of disappearing polymorphs has been described extensively by Dunitz and Bernstein,<sup>9</sup> who detail the common causes and problems. Examples of such occurrences are taken almost exclusively from the field of organic rather than coordination chemistry, most likely for the reasons mentioned above. A well-documented case is that of 1,2,3,5-tetra-*O*-acetyl- $\beta$ -D-ribofuranose,<sup>10</sup> for which metastable polymorph A was first prepared in 1947; it “disappeared” in 1954 following the discovery of the higher-melting polymorph B. Polymorph A was then irreproducible across numerous countries until 1981, when scientists in Budapest were able to recover it,<sup>11</sup> presumably because their laboratory had remained free from contamination by the more stable B form. One particularly high-profile case was that of Ritonavir which is prescribed as an anti-HIV medication: two years after it was introduced, the formation of a more stable polymorph with lower solubility and bioavailability led to its temporary withdrawal from sale.<sup>12</sup>

One method used for polymorph control is epitaxy, whereby another surface is used to promote the growth of a given phase or orientation of a crystal. The technique is employed to obtain the correct polarity of GaN for electronics<sup>13</sup> and to attach metal–organic frameworks to surfaces,<sup>14</sup> typically using surfaces of a different chemical composition to that of the desired product; in these examples, sapphire and gold are typically used, respectively. Elsewhere, Braga et al. employed the seeding effect of a powder of the desolvated hydrate phase of  $[\text{Co}^{\text{III}}(\eta^5\text{-C}_5\text{H}_4\text{COOH})(\eta^5\text{-C}_5\text{H}_4\text{COO})]$  to directly yield otherwise unobtainable single crystals of the nonsolvated phases<sup>15</sup> and, using a single crystal of pimelic acid, Ward et al. showed that the so-called “YN” (yellow-needle) metastable phase of 5-methyl-2-[(2-nitrophenyl)amino]-3-thiophenecarbonitrile can also be obtained by epitaxy,<sup>16</sup> but only on the (101) faces of the substrate. Rather counterintuitively, it has also been observed that in some cases the stable phase of a compound will bring about growth of the metastable phase during crystal growth, for example, with sulfathiazole<sup>17</sup> and the steroid reported by Stoica et al.<sup>18</sup> Polymer heteronuclei may also be used to control polymorphism<sup>19</sup> and the technique has been demonstrated on a variety of organic compounds.<sup>20</sup> Clearly, seeding and epitaxy offer an appealing solution to the challenge of obtaining metastable polymorphs. In most reported examples it appears that the substrates used differ significantly from the desired phase, but if an isomorphous system of a compound chemically similar to a lost phase were to exist then this would be an obvious candidate. For any such approach to be viable, the seed phase also needs to be stable to the recrystallization conditions, for example, by being insoluble in the solution used.

As an extension of our investigations into the unusual properties of thioether macrocycle complexes,<sup>21–23</sup> we have studied complexes of analogous oxathioether macrocycles. While studying  $[\text{PdCl}_2([\text{9}]\text{aneS}_2\text{O})]$  ( $[\text{9}]\text{aneS}_2\text{O}$  = 1-oxa-4,7-dithiacyclononane), **1**, two previously unreported phases, designated  $\beta$ -**1** and  $\gamma$ -**1**, were discovered: the preparation of the first of these to be revealed ( $\beta$ -**1**) could not be reproduced

following discovery of the  $\gamma$ -**1** form and it was therefore eventually designated as a disappearing polymorph. The previously unreported analogous complex  $[\text{PtCl}_2([\text{9}]\text{aneS}_2\text{O})]$ , **2**, was also investigated and a phase suitable for the epitaxial retrieval of the disappearing polymorph  $\beta$ -**1** was identified. We report herein these new crystallographic phases and discuss the potential causes of the instability of  $\beta$ -**1** with reference to structural characteristics and DFT calculations.

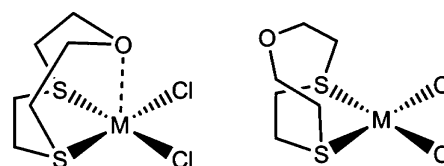
## EXPERIMENTAL SECTION

**Synthesis.** Reagents were used as received from Sigma-Aldrich, Fischer Industries, Acros Organics, Alfa Aesar, and Merck Schuchardt. NMR spectroscopy was carried out at 400 MHz using Bruker AV400 and Bruker AV(III)400 spectrometers. IR spectroscopy was carried out using a Bruker Tensor 27 FTIR or ThermoScientific Nicolet iS5 FTIR with an iD5 ATR attachment. ESI mass spectrometry was undertaken using a Bruker Daltonics microTOF electrospray mass spectrometer and MALDI mass spectrometry using a Bruker Ultraflex III spectrometer equipped with a matrix-assisted laser desorption ionization source and used a DTCB matrix. Elemental analysis was undertaken using an Exeter Analytical CE-440 Elemental Analyzer.

**1-Oxa-4,7-dithiacyclononane** ( $[\text{9}]\text{aneS}_2\text{O}$ ). Dimethylformamide (500 mL) was added to  $\text{Cs}_2\text{CO}_3$  (16.9 g, 87.6 mmol) and heated to 100 °C. Under vigorous stirring, solutions of mercaptoethyl ether (4.5 mL, 36 mmol) and dibromoethane (3.2 mL, 37 mmol) in dimethylformamide (40 mL, 40 mL) were added dropwise at a rate of 1.2 mL per hour. After addition, the solution was allowed to cool and thereafter was stirred for 3 days. The resulting suspension was filtered and the volume reduced in vacuo to yield a yellow/brown oil that solidified after repressurization. This oil was dissolved in  $\text{CH}_2\text{Cl}_2$  (100 mL) and washed with water (2  $\times$  50 mL), aqueous NaOH (0.1 M, 4  $\times$  50 mL), and water again (4  $\times$  50 mL). Excess  $\text{MgSO}_4$  was added and the suspension stirred overnight. The product was purified by Kugelrohr distillation as the first fraction and yielded a colorless oil (1.668 g, 10.15 mmol, yield 28%). Mass spectrometry (ESI, MeCN): 187 ( $M + \text{Na}$ )<sup>+</sup>. <sup>1</sup>H NMR  $\delta_{\text{H}}$ /ppm (400 MHz;  $\text{CD}_3\text{CN}$ ): 2.75 (4H, t, <sup>2</sup> $J_{\text{HH}}$  = 4.0 Hz,  $\text{CH}_2$ ), 3.00 (4H, s,  $\text{CH}_2$ ), 3.68 (4H, t, <sup>2</sup> $J_{\text{HH}}$  = 4.0 Hz,  $\text{CH}_2$ ). <sup>13</sup>C NMR  $\delta_{\text{C}}$ /ppm (400 MHz;  $\text{CD}_3\text{CN}$ ): 34.31 (*sp*<sup>3</sup>C), 35.90 (*sp*<sup>3</sup>C), 74.95 (*sp*<sup>3</sup>C). Anal. Calcd for  $\text{C}_6\text{H}_{12}\text{OS}_2$ : C = 43.86, H = 7.36, N = 0%. Found: C = 43.65, H = 7.30, N = 0%. IR  $\nu/\text{cm}^{-1}$  ( $\text{CHCl}_3$ ): 3006 (s), 2958 (s), 2919 (s), 2862 (s), 1465 (w), 1410 (s), 1361 (w), 1295 (s), 1274 (s), 1255 (w), 1149 (w), 1113 (s, br), 1043 (w), 1023 (w), 1007 (w), 911 (w).

**$[\text{PdCl}_2([\text{9}]\text{aneS}_2\text{O})]$  - **1**.** 1-Oxa-4,7-dithiacyclononane (150 mg, 0.91 mmol) in MeCN (15 mL) was added to a suspension of  $\text{PdCl}_2$  (142 mg, 80 mmol) in MeCN (10 mL) and stirred for 30 min before filtering. The solids were washed with MeCN (10  $\times$  5 mL), the washings combined with the mother liquor and the volume reduced in vacuo (~10 mL).  $\text{Et}_2\text{O}$  (40 mL) was added slowly, causing a bright orange powder to precipitate. This was obtained by filtration and dried in air (97.4 mg, 0.28 mmol, yield 35%). Mass spectrometry (ESI, MeCN): 341  $M^+$ . Anal. Calcd for  $\text{C}_6\text{H}_{12}\text{Cl}_2\text{OPdS}_2$ : C = 21.1, H = 3.54, N = 0%. Found: C = 20.96, H = 3.36, N = 0%. IR  $\nu/\text{cm}^{-1}$  (ATR): 2972 (w), 2934 (w), 2873 (w), 1489 (w), 1467 (w), 1423 (w), 1414 (w), 1400 (w), 1299 (w), 1282 (w), 1227 (w), 1195 (w), 1140 (w), 1122 (s), 1056 (w), 1018 (m), 1003 (m), 921 (m), 805 (w), 787 (w).

**Scheme 1. Scheme Showing Endodentate (Left) and Exodentate (Right) Conformers of  $[\text{MCl}_2([\text{9}]\text{aneS}_2\text{O})]$  (**1**, M = Pd; **2**, M = Pt)**



[PtCl<sub>2</sub>([9]aneS<sub>2</sub>O)]- **2**. 1-Oxa-4,7-dithiacyclononane (75 mg, 46 mmol) in MeCN (5 mL) was added to a solution of PtCl<sub>2</sub> (106 mg, 0.400 mmol) in MeCN (20 mL) and the suspension stirred at 60 °C for 19 h. Upon cooling, a green precipitate formed which was collected by filtration, washed with Et<sub>2</sub>O (4 × 2 mL) and dried in air (124 mg, 0.287 mmol, yield 72%). Mass spectrometry (ESI, MeCN): 453 (M + Na)<sup>+</sup>. Anal. Calcd for C<sub>6</sub>H<sub>12</sub>Cl<sub>2</sub>OPtS<sub>2</sub>: C = 16.7, H = 2.81, N = 0%. Found: C = 16.69, H = 2.66, N = 0%. IR  $\nu$ /cm<sup>-1</sup> (ATR): 2972 (w), 2930 (w), 2873 (w), 1485 (w), 1464 (w), 1422 (w), 1412 (w), 1399 (w), 1300 (w), 1281 (w), 1228 (w), 1194 (w), 1141 (w), 1125 (s), 1056 (w), 1018 (m), 1001 (m), 916 (m), 803 (w), 787 (w).

**Recrystallizations.** Saturated solutions of **1** and **2** were prepared by stirring excess compound in MeNO<sub>2</sub> overnight at 35 °C before allowing the solution to cool and residual solid to settle. Vapor diffusion recrystallizations were then carried out using the decanted saturated solutions with Et<sub>2</sub>O as the antisolvent. These were carried out at room temperature (15–20 °C) to give the  $\alpha$  phases and the nonepitaxially obtained  $\beta$ -1 (vide infra). Recrystallization at 25, 30, or 35 °C yielded  $\gamma$ -1 and  $\beta$ -2 from their respective solutions. In all cases, these recrystallizations were attempted using either the saturated solution or diluted concentrations (75%, 50%, or 25%) thereof; crystal growth rates were controlled by varying the number of apertures in the lid of the vessel containing the solution of **1** or **2**, using either standard 0.5 dram glass vials or NMR tubes: the temperature appeared to be the only variable that affected which phase was obtained.

For the epitaxial growth experiments, a crystal of  $\beta$ -2 was fixed to a glass capillary using the minimum amount of epoxy resin. The crystal was held just above the surface of a saturated solution of **1** in MeNO<sub>2</sub> and a vapor diffusion recrystallization using Et<sub>2</sub>O as the antisolvent was carried out. Crystals obtained were broken off and analyzed using single crystal X-ray diffraction, or dissolved in MeNO<sub>2</sub> for MALDI mass spectrometry (vide infra). The same procedure was also carried out using  $\gamma$ -1 as the seed, either with saturated solutions of **2** or with solutions which were saturated first with **2** and then with **1**.

**Crystallography.** All crystallographic experiments were undertaken at 293 K on an Agilent SuperMova system using mirror-monochromated Mo K $\alpha$  radiation ( $\lambda = 0.71073$  Å) detected at an Eos CCD area detector. Data reduction and refinement were carried out using Agilent CrysAlisPro software.<sup>24</sup> Numerical absorption corrections based on Gaussian integration over a multifaceted crystal model were applied. Structure solutions were obtained using SHELXS direct methods and refined using SHELXL<sup>25</sup> through Olex2.<sup>26</sup> Experimental tables can be found in the Supporting Information.

**Computational Methods.** The relative total energies and cohesive energies (CEs) of the five phases revealed in this study, as well as those for a hypothetical third phase of **2** (designated  $\gamma$ -2) which is isomorphous and isostructural with  $\gamma$ -1, were calculated using density functional theory (DFT) with on-the-fly ultrasoft pseudopotentials and the Perdew–Burke–Ernzerhof (PBE)<sup>27</sup> exchange–correlation functional, as implemented in the CASTEP code.<sup>28</sup> A plane-wave basis set with an energy cutoff of 800 eV was used for the valence electron wave functions. The Brillouin zone was sampled within the Monkhorst–Pack scheme<sup>29</sup> using a (3 × 3 × 3)  $\Gamma$ -centered  $k$ -points grid. To account for the dispersion interactions between molecules in the crystal, the semiempirical methods of Grimme<sup>30</sup> and Tkatchenko–Scheffler<sup>31</sup> were examined. The initial atomic coordinates and lattice parameters for the investigated polymorphs were taken from the crystallographic data obtained in this study. The lattice parameters and atomic positions were subsequently optimized for each polymorph structure. Calculated values for selected structural and lattice parameters are provided in the Supporting Information (Tables A1 and A2).

## RESULTS AND DISCUSSION

**Crystallization of Complexes.** Diffusion of Et<sub>2</sub>O vapor into a saturated solution of **1** in MeNO<sub>2</sub> at 15–20 °C yielded clear orange blocky crystals primarily of the phase  $\alpha$ -1.  $\beta$ -1 was initially obtained as the minor product of the aforementioned recrystallization, and were separate from the bulk of the crystals

which were located lower in the vial. Repetition of these conditions yielded only  $\alpha$ -1. All further efforts to yield the  $\beta$ -1 phase gave either  $\alpha$ -1 or a second previously unreported phase designated  $\gamma$ -1 with higher recrystallization temperatures favoring the latter. Crystals of  $\alpha$ -2 were obtained by diffusion of Et<sub>2</sub>O vapor into a saturated solution of **2** in MeNO<sub>2</sub> at 15–20 °C, while  $\beta$ -2 was obtained by performing these recrystallizations at elevated temperatures of 30 or 35 °C.

Orange block-shaped crystals of  $\beta$ -1 were grown epitaxially using a pale green seed crystal of  $\beta$ -2 (Figure 1). The crystals were readily separated from the seed crystal and were identified (vide infra) as being of the same phase as the original crystals ( $\beta$ -1) and designated  $\beta$ -1-epitaxy to distinguish them from the original crystals of this phase. Crystals appeared to grow from all exposed faces of the seed crystal rather than from any one in particular.

Attempts to use the same technique to obtain crystals of the hypothetical  $\gamma$  phase of **2** using a saturated solution of **2** and crystals of  $\gamma$ -1 were unsuccessful, resulting in the dissolution of the seed crystal and the recovery of  $\alpha$ -2. The use of a solution which had been sequentially saturated in **2** and **1** yielded the same result.

**Crystal Structures.** Detailed structural reports of the new complexes and phases discovered during this study, namely,  $\beta$ -1,  $\gamma$ -1,  $\alpha$ -2, and  $\beta$ -2, along with details of the structure of  $\alpha$ -1 reported previously<sup>32</sup> are given in Supporting Information. Relevant structural features of the phases for the discussion are reported below and in all cases  $Z' = 1$ .

Complexes  $\alpha$ -1 and  $\alpha$ -2 are isomorphous and isostructural with one another and crystallize in the monoclinic space group  $P2_1/n$ . In these phases the macrocycle adopts an *endodontate* conformation with respect to the oxygen donor, yielding an additional apical M...O interaction [Pd...O = 2.958(4) Å; Pt...O = 3.077(4) Å] to the *cis*-Cl<sub>2</sub>S<sub>2</sub> square planar coordination of the metal centers. The M...O distances lie within the sum of the relevant van der Waals radii (3.15 Å for  $\alpha$ -1, 3.27 Å for  $\alpha$ -2).<sup>33</sup> Molecules pack into dimers [for  $\alpha$ -1, Pd...Pd = 3.7903(10) Å; for  $\alpha$ -2, Pt...Pt = 3.8237(4) Å] (Figure 2) with the coordination planes parallel to each other and with perpendicular separations of the least-squares planes of 3.625(2) and 3.6815(14) Å and shifts of 1.182(2) and 1.120(2) Å for  $\alpha$ -1 and  $\alpha$ -2, respectively. These dimers form ABAB alternating sheets in the *bc* plane, generating a

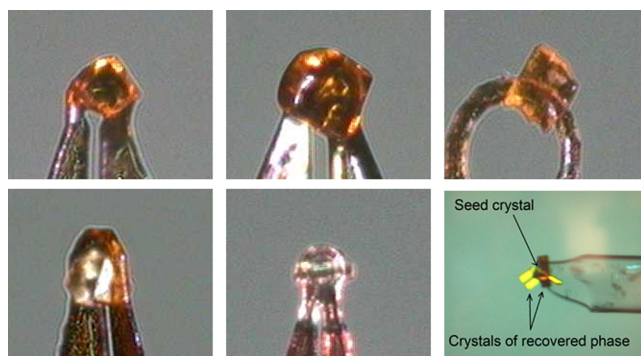


**Figure 1.** (From left to right, top to bottom) Pictures of  $\alpha$ -1,  $\beta$ -1,  $\gamma$ -1,  $\alpha$ -2, and  $\beta$ -2 on MicroMounts, and crystals of  $\beta$ -1 grown epitaxially on a seed crystal of  $\beta$ -2 stuck to a glass capillary tube viewed with polarized light. All phases have been observed as growing as rods, plates, and blocks, with the only difference between them being that phases of **1** are deep orange and phases of **2** are pale green in color.

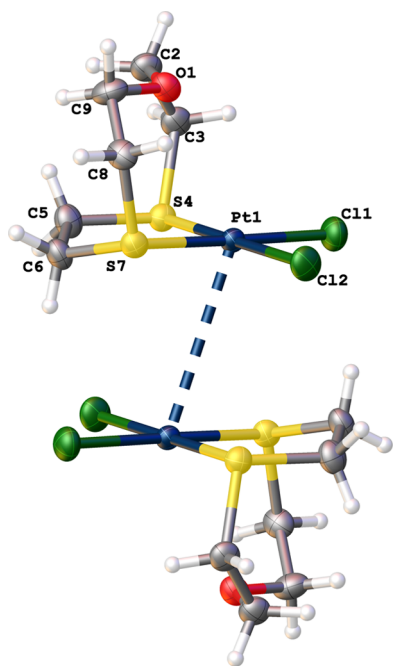


**Figure 2.** View of the dimer formed in the structure of  $[\text{PtCl}_2([\text{9}] \text{aneS}_2\text{O})]$  in  $\alpha$ -2. Displacement ellipsoids are shown at 50% probability. Phases  $\alpha$ -1 and  $\alpha$ -2 are isostructural.

herringbone-like pattern when viewed along the  $a$  axis (Figure 3).

The  $\beta$ -1 and  $\beta$ -2 polymorphs are also isomorphous and isostructural, forming in monoclinic space group  $P2_1/c$ , and are conformationally distinct from their respective  $\alpha$  phases. The macrocycle in each  $\beta$  polymorph adopts an *exodentate* conformation with respect to the oxygen donor: the resulting  $\text{M}\cdots\text{O}$  distances [ $\text{Pd}\cdots\text{O} = 3.404(3)$  Å;  $\text{Pt}\cdots\text{O} = 3.450(2)$  Å] indicate the absence of any significant apical  $\text{M}\cdots\text{O}$  interaction to supplement the *cis*- $\text{Cl}_2\text{S}_2$  square planar coordination of the metal center. As in the  $\alpha$  phases, molecules in the  $\beta$  phases form

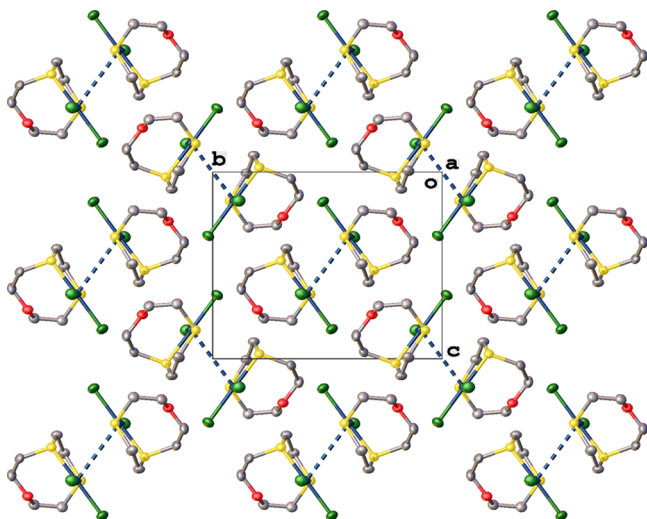


**Figure 3.** View of the herringbone packing of  $[\text{PtCl}_2([\text{9}] \text{aneS}_2\text{O})]$  dimers in  $\alpha$ -2 viewed along the  $a$  axis. Intermolecular  $\text{Pt}\cdots\text{Pt}$  interactions are highlighted with dashed bonds, hydrogen atoms omitted for clarity, and displacement ellipsoids shown at 50% probability. Phases  $\alpha$ -1 and  $\alpha$ -2 are isostructural.

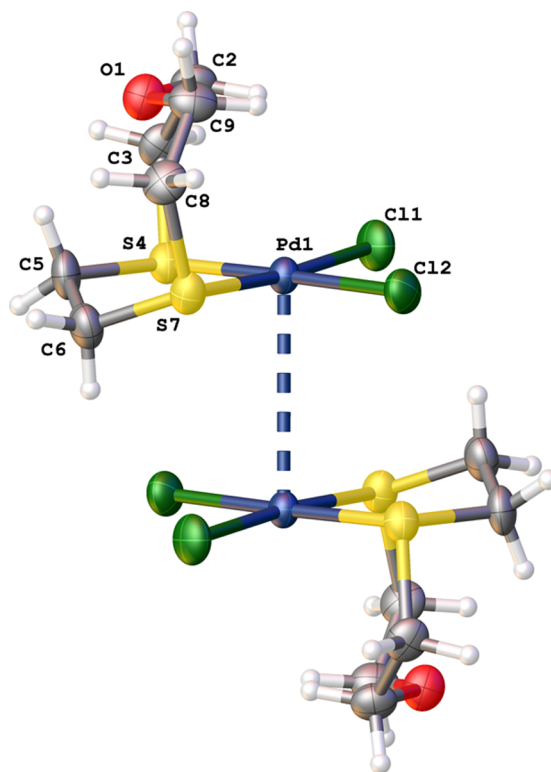


**Figure 4.** View of the dimers formed between molecules of  $[\text{PdCl}_2([\text{9}] \text{aneS}_2\text{O})]$  in  $\beta$ -1. Displacement ellipsoids shown at 50% probability.  $\beta$ -2 and  $\beta$ -1 are isostructural.

dimers [for  $\beta$ -1,  $\text{Pd}\cdots\text{Pd} = 3.4946(7)$  Å; for  $\beta$ -2,  $\text{Pt}\cdots\text{Pt} = 3.5294(2)$  Å] (Figure 4) with coordination planes parallel to one another, but with decreased perpendicular separation and a shift of the least-squares planes compared to the  $\alpha$  phase structures [for  $\beta$ -1, 3.5237(11) and 0.417(2) Å; for  $\beta$ -2, 3.5471(6) and 0.4003(11) Å, respectively]. These pack into sheets in the  $bc$  plane with the intradimer  $\text{M}\cdots\text{M}$  vector aligned approximately parallel to the  $a$  axis, affording alternating hydrophilic and hydrophobic layers (Figure 5).

In  $\gamma$ -1, which forms in monoclinic space group  $P2_1/n$ , the *exodentate* conformer is again observed, the  $\text{Pd}\cdots\text{O}$  separation of 3.378(3) Å indicating that there is no significant apical  $\text{M}\cdots\text{O}$  interaction. The molecules do not form dimers in the solid state, but each *exodentate* O donor is directed toward the base of a neighboring molecule. The resulting intermolecular  $\text{Pd}\cdots\text{O}$  interactions [ $\text{Pd}\cdots\text{O}^i = 3.212(3)$  Å] link molecules into chains that run parallel to the  $b$  axis (Figure 6) and can be designated as  $C(5)$  following graph set analysis;<sup>34</sup> a  $\text{C}-\text{H}\cdots\text{Cl}$  intermolecular hydrogen bond [ $\text{Cl2}\cdots\text{H3B}^i = 2.87$  Å,  $\text{Cl2}\cdots\text{H3B}^i-\text{C3}^i = 165^\circ$ ; symmetry code  $i: 0.5 - x, -0.5 + y, 1.5 - z$ ] also appears in this formation and both interactions lie within the sum of the relevant van der Waals radii (3.15 and 2.95 Å, respectively).<sup>33</sup>

**Similarity between the  $\alpha$  and  $\beta$  Phases.** The molecules pack as similar dimeric units in the  $\alpha$  and  $\beta$  phases. In the  $\alpha$  phase, these form a herringbone-like array, whereas in the  $\beta$  phases they align and pack into sheets. Despite this difference the two modes of packing are very similar, although a packing overlay routine using Mercury<sup>35</sup> gives only a 5/15 molecule match using default parameters. An overlay of the phases viewed along the co-parallel  $b$  axes (Figure 7) shows their relation to one another. Where the overlap of the dimers at site

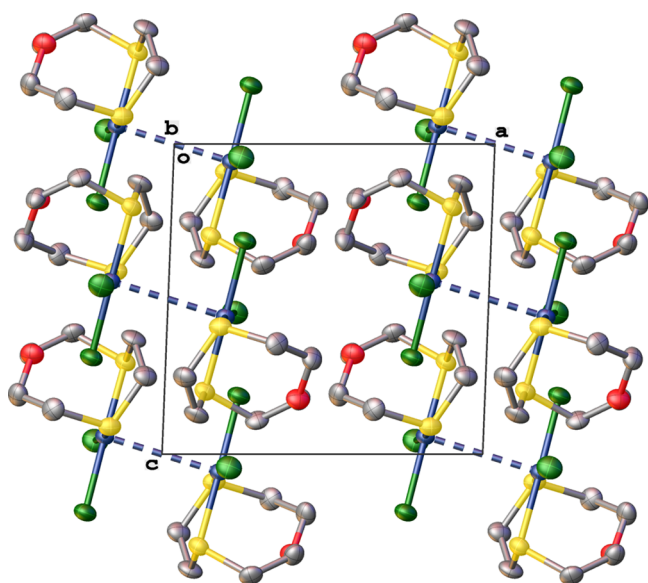


**Figure 5.** View of the layered packing of dimers of  $[\text{PdCl}_2([\text{9}] \text{aneS}_2\text{O})]$  in  $\beta$ -1, showing two layers running perpendicular to the  $a$  axis. Intermolecular Pd...Pd interactions are highlighted with dashed bonds, hydrogen atoms are omitted for clarity and displacement ellipsoids shown at 50% probability. The phases  $\beta$ -2 and  $\beta$ -1 are isostructural.

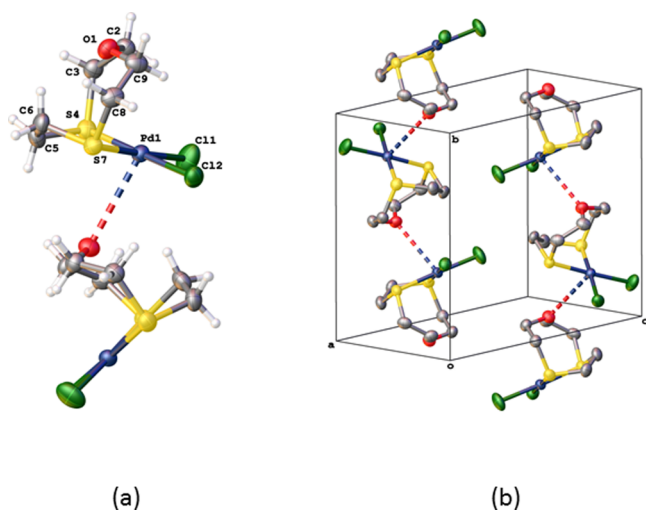


**Figure 6.** View of (a) the chain formation and (b) the unit cell of  $[\text{PdCl}_2([\text{9}] \text{aneS}_2\text{O})]$  in  $\gamma$ -1. Intermolecular Pd...O interactions are highlighted using dashed bonds, hydrogen atoms are omitted for clarity in (b) and displacement ellipsoids shown at 50% probability.

$I$  is maximized, half the dimers can be seen as having rotated through  $90^\circ$  about the  $z$  axis, as defined, when moving from the  $\beta$  to  $\alpha$  phase. This allows the dimers that remain aligned to  $I$  to move along the  $y$  axis and toward  $I$ . Little displacement is observed along the  $x$  and  $z$  axes, resulting in denser packing of molecules.

A destructive phase transition was observed upon cutting a crystal of  $\beta$ -1 which transformed its lattice to multiple  $\alpha$ -1 lattices. Although the supramolecular dimeric motif is retained across the two phases, this change in packing is accompanied by a change in the conformation of the molecule from *exodentate* to *endodentate*. There is little evidence to indicate the order in which these events occur, but both the conformational change

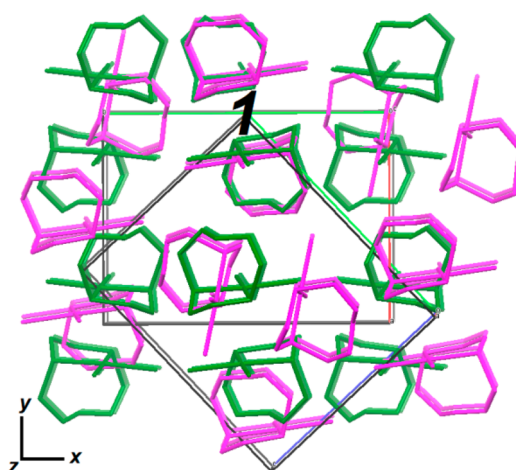


**Figure 7.** A ca. two-cell deep packing overlay of  $\alpha$ -1 (magenta) and  $\beta$ -1 (green), optimized for the overlay of dimers at site  $I$ . Hydrogen atoms are omitted for clarity.

and rotation of the dimeric arrangements would significantly alter the intermolecular interactions about the molecule: one could potentially lead to the other, or they could occur concomitantly.

**Computational Results.** DFT calculations with dispersion corrections were carried out using CASTEP<sup>28</sup> to obtain total electronic energies and cohesive energies of the investigated polymorphic structures. The dispersion interactions were added using semiempirical methods of Grimme<sup>30</sup> (G06) and Tkatchenko-Sheffler<sup>31</sup> (TS). The DFT-G06 and DFT-TS energies returned for **1** were comparable to within 0.005% and the difference between the energies of the phases was only marginally greater with DFT-G06. Table 1 shows the DFT-TS relative total energies and cohesive energies (per molecule) of different phases of polymorphs **1** and **2**. The values of the total energy are shown relative to the most stable  $\alpha$ -phases. The cohesive energy is defined as the difference between the total energy of the crystalline material at equilibrium (per molecule) and the energy of a free molecule in its ground state. Geometry optimization of individual molecules has been performed in a cubic supercell with dimensions of 20 Å. Partial atomic charges have been determined from the Mulliken population analysis and are provided in the Supporting Information (Table A3).

**Phase Loss and Retrieval.** A very small number of crystals of the previously unreported phase  $\beta$ -1 were originally recrystallized in the upper region of a vial, the lower part of which contained a mass of crystals identified as  $\alpha$ -1. Our attempts to cut crystals of  $\beta$ -1 induced an incomplete  $\beta \rightarrow \alpha$  phase transformation. The resulting diffraction pattern comprised multiple components, with 90% of reflections

**Table 1.** Relative Total Energies,  $\Delta E$ , and Cohesive Energies, CE, of Different Phases of Polymorphs **1** and **2**<sup>a</sup>

phase	$\Delta E$ , kJ mol <sup>-1</sup>	CE, kJ mol <sup>-1</sup>
$\alpha$ -1	0	225.29
$\beta$ -1	7.43	188.92
$\gamma$ -1	8.01	188.34
$\alpha$ -2	0	226.26
$\beta$ -2	8.59	188.92
" $\gamma$ -2"	11.19	186.41

<sup>a</sup>The zero energy is assigned to the most stable  $\alpha$ -phase in each case.

Table 2. Unit Cell Parameters for  $\beta$ -1 and  $\beta$ -2 Showing Their Close Phase Match<sup>a</sup>

phase	<i>a</i> /Å	<i>b</i> /Å	<i>c</i> /Å	$\beta$ /°	<i>V</i> /Å <sup>3</sup>
$\beta$ -1	9.3384(3)	12.6575(4)	9.0498(3)	92.260(3)	1068.87(6)
$\beta$ -2	9.4167(2)	12.6646(2)	9.0376(2)	91.530(2)	1077.43(3)
$\beta$ -1-epitaxy	9.3451(4)	12.6701(5)	9.0724(4)	92.424(4)	1073.25(8)

<sup>a</sup>Also shown are the unit cell parameters for  $\beta$ -1-epitaxy.

Table 3. Selected Parameters for the Structure Refinement of  $\beta$ -1-epitaxy Using Different Ratios of Pd:Pt in Absorption Correction

% Pd:Pt	$R_{\text{int}}$	final $R_1$ [ $I \geq 2\sigma(I)$ ]	final $wR_2$ [ $I \geq 2\sigma(I)$ ]	<i>S</i>	$e^-$ max/ $e \text{ \AA}^{-3}$	$e^-$ min/ $e \text{ \AA}^{-3}$	no of restraints
0:100	0.0233	0.1174	0.3544	1.574	9.14	−4.68	100
50:50	0.0236	0.0768	0.2429	1.083	3.88	−2.13	124
75:25	0.0236	0.0528	0.1598	1.064	1.41	−1.22	2
90:10	0.0234	0.0398	0.1011	1.074	0.67	−0.85	0
100:0	0.0234	0.0336	0.0603	1.024	0.49	−0.59	1

indexing to six components all identified as  $\alpha$ -1, 4% to a single  $\beta$ -1 lattice, and the remaining 6% unindexed. In view of this interesting phenomenon, further crystals of  $\beta$ -1 were sought in order to investigate it further.

It had already been established that the temperature of the laboratory in which the crystals were originally obtained could fluctuate significantly during the day. The distinctive location of  $\beta$ -1 crystals in the upper part of the vial suggested that they grew in the later stages of the experiment following the influx of antisolvent, and on this basis a number of tentative inferences were made. It is possible that the temperature of the sample varied with the temperature of the surroundings, resulting in the dissolution and subsequent recrystallization of a small amount of material at higher temperatures: in these circumstances, the relative concentrations of complex, solvent, and antisolvent present in the system could be significantly different from those for the recrystallization of  $\alpha$ -1. The hypothesis of the temperature and solvent environment playing a key role in the crystallization of these two conformational polymorphs was supported by work carried out by Lucas et al., who showed using temperature-dependent NMR that, when dissolved in DMSO, an increase in temperature brings about an increase in fluxionality in the macrocycle of **1** that is not seen when the experiment is carried out in nitrobenzene.<sup>32</sup> An additional consideration in phase growth is that there could have been an unknown seed crystal present in the recrystallization vial that may have acted as a nucleation site. Consequently, three factors were considered as potentially affecting the phase obtained: the temperature of the recrystallization medium, the relative concentrations of the components, and the presence of seed crystals.

To test for location-dependent seeding affects, a possibility discussed by Dunitz and Bernstein,<sup>9</sup> ambient temperature recrystallizations by vapor diffusion were undertaken in a number of different laboratories in the same building, including the one in which the original result was obtained: all yielded only the  $\alpha$ -1 phase. To investigate the effect of temperature on the system, similar recrystallizations were carried out at 30 and 35 °C, yielding crystals of the new phase  $\gamma$ -1, occasionally accompanied by crystals of  $\alpha$ -1. Variation of the concentration of the starting solution by dilution of the saturated solution was attempted for all temperatures but there were no systematic effects on the outcome of the recrystallization. Noting the similarity between  $\alpha$ -1 and  $\beta$ -1, we speculated that the presence of a seed crystal of  $\alpha$ -1 might help to seed the growth of  $\beta$ -1.

Recrystallizations were therefore set up which replicated the temperature fluctuations that could have occurred during the original recrystallization after the formation of some  $\alpha$ -1, but these attempts yielded only crystals of  $\alpha$ -1,  $\gamma$ -1, or a mixture of the two phases. Recrystallization of **2** by vapor diffusion at ambient temperature yielded crystals of  $\alpha$ -2, while at 30 or 35 °C these experiments yielded either  $\alpha$ -2 or, more commonly, a combination of both  $\alpha$ -2 and  $\beta$ -2 phases. None of our experiments yielded crystals of the hypothetical  $\gamma$ -2 phase.

The solubility of complex **2** in MeNO<sub>2</sub> was found to be significantly lower than that of **1** and, combined with the close phase match of  $\beta$ -1 and  $\beta$ -2 (Table 2), led us to the conclusion that it should be possible to grow a crystal of  $\beta$ -1 directly on a crystal of  $\beta$ -2 using epitaxial techniques. By the end of this experiment, the pale green seed crystal was surrounded by protrusions of deep orange single crystals (see Figure 1) which were readily separated from the seed crystal (and designated  $\beta$ -1-epitaxy to distinguish them from the original  $\beta$ -1 crystals). The experiment also yielded crystals identified as  $\alpha$ -1 which had grown conventionally on the walls of the vessel.

Crystals of  $\beta$ -1-epitaxy were characterized by MALDI mass spectrometry and single crystal X-ray diffraction to ascertain whether there was any residual contamination by  $\beta$ -[PtCl<sub>2</sub>([9]-aneS<sub>2</sub>O)], either by solid-state diffusion or via partial dissolution of the seed material in the recrystallization solution. Mass spectrometry revealed peaks with isotope patterns corresponding to the Pd(II) complex, but none from the Pt(II) complex. Data from one ambient-temperature data collection were reanalyzed using varying proportions of Pd and Pt for the absorption correction, and structure solution and refinement of the metal site was in each case carried out. No reflections were omitted, no application of further extinction correction was carried out and refinement was undertaken using only distance restraints on 1,2-bonded distances and rigid-bond restraints on anisotropic displacement parameters where necessary. The structures were refined to convergence and the results clearly indicate an absence of Pt in the system (Table 3).

Comparison of the unit cell parameters (Table 2) of the epitaxially grown crystals with those of  $\beta$ -2 and the original  $\beta$ -1 showed a considerably closer correspondence with the latter. Similarly, comparison of intradimer parameters for  $\beta$ -1-epitaxy show close matches with those of  $\beta$ -1 (Table 4).

Although the M–S and M–Cl bond lengths do not differ greatly between  $\beta$ -1 and  $\beta$ -2, and so do not provide effective

**Table 4.** Basic Parameters for the Comparison of the Intradimer Geometry in the Epitaxially Recovered Phase  $\beta$ -1-epitaxy with  $\beta$ -1 and  $\beta$ -2<sup>a</sup>

structure	centroid-centroid /Å	perpendicular separation /Å	shift /Å
$\beta$ -1	3.5483(11)	3.5237(10)	0.4171(14)
$\beta$ -2	3.5696(6)	3.5471(6)	0.4003(11)
$\beta$ -1-epitaxy	3.5497(9)	3.5258(9)	0.411(2)

<sup>a</sup>Note that the data for  $\beta$ -1-epitaxy fit most closely with those for  $\beta$ -1.

discrimination, the intermolecular M...M and intramolecular M...O separations vary more significantly and therefore provide a clear indicator of the metal present in the crystal. M...M and M...O distances in  $\beta$ -1-epitaxy are identical to those in  $\beta$ -1 to within 1 s.u. but differ greatly from those in  $\beta$ -2 (Table 5). We therefore conclude that  $\beta$ -1-epitaxy represents a successful recovery of the previously "lost"  $\beta$ -1 phase, whereby the isomorphous and isostructural nature of  $\beta$ -2 provides a sufficiently complementary interaction set to favor nucleation of the phase on its surface.

**Phase Stabilities.** The relative stabilities of polymorphs can be inferred from their crystal densities.<sup>36</sup> For molecular crystals, it is generally the case that the densest phase will be the most thermodynamically stable, and the densities of the phases can be readily calculated from crystallographic data (Table 6). From these values, it can be inferred that the  $\alpha$  phases are significantly more thermodynamically stable than the  $\beta$  phases, and  $\gamma$ -1 marginally more stable than  $\beta$ -1. The densities calculated from the DFT-TS optimized structures (Table 6) are in a good agreement with those derived from the experimentally determined structures and corroborate the same trend.

Comparison of the total energies calculated for each phase (Table 1) confirms that the *endodentate*  $\alpha$  phases are significantly more stable than the *exodentate* phases. It was found that the energy per molecule of  $\beta$ -1 is 7.43 kJ mol<sup>-1</sup> higher than that of  $\alpha$ -1, and for  $\gamma$ -1 it further increased by 0.58 kJ mol<sup>-1</sup> in contrast to the order inferred from the crystal densities and the observation that  $\gamma$ -1 is the preferred *exodentate* modification of 1. The calculated energy difference between  $\beta$ -1 and  $\gamma$ -1 is, however, too small to make any firm conclusions about the relative stability of these two phases owing to the possible errors associated with the approximations adopted in the computational method.

Given the structural similarities and the energies of the phases, the appearance of a  $\beta \rightarrow \alpha$  phase transformation in a crystal of  $\beta$ -1 is perhaps unsurprising. The existence of such a phase transition in the hindered environment of a macroscopic single crystal suggests that the barrier for this transformation is relatively low. Therefore, it is reasonable to suggest that  $\beta$ -1 is not seen because it would be favorable for it to relax to  $\alpha$ -1 in the early stages of crystal growth. As the energies are so similar for  $\gamma$ -1 and  $\beta$ -1, the observation of  $\gamma$ -1 seems less surprising. It is also worth noting that the *exodentate* conformation of the macrocycle in  $\gamma$ -1 gives rise to specific intermolecular O...Pd

**Table 6.** Densities (g cm<sup>-3</sup>) of the Various Phases Taken from Experimentally Determined and DFT-TS Optimized Structures

phase	conformation	experimental	computational
$\alpha$ -1	<i>Endodentate</i>	2.201	2.176
$\beta$ -1	<i>Exodentate</i>	2.123	2.115
$\gamma$ -1	<i>Exodentate</i>	2.133	2.121
$\alpha$ -2	<i>Endodentate</i>	2.763	2.733
$\beta$ -2	<i>Exodentate</i>	2.653	2.660
" $\gamma$ -2"	<i>Exodentate</i>	n/a	2.659

and C-H...Cl interactions that are not observed in  $\beta$ -1 and may stabilize the *exodentate* conformer during growth of  $\gamma$ -1 via electrostatic attractions given the favorable partial atomic charges (Table A3 of Supporting Information). This, coupled with there being no evidence of a route for it to convert to the stable  $\alpha$  phase, would provide a rationale as to why  $\gamma$ -1 is observed when  $\beta$ -1 is not.

In the case of  $\beta$ -2, which was the only *exodentate* modification of 2 obtained in the study, the total energy was found to be 8.59 kJ mol<sup>-1</sup> higher than  $\alpha$ -2. A calculation on a hypothetical phase of 2, which is isomorphous and isostructural to  $\gamma$ -1 and is designated  $\gamma$ -2, yielded an energy 2.6 kJ mol<sup>-1</sup> higher than  $\beta$ -2. The total difference in energy of 11.19 kJ mol<sup>-1</sup> between  $\alpha$ -2 and  $\gamma$ -2 suggests that the latter is not observed as it is less favored thermodynamically.

The cohesive energies (CEs) were also calculated for these systems (Table 1) and these again found the  $\alpha$  phases to be the most thermodynamically favorable, with CEs of 225.29 and 226.26 kJ mol<sup>-1</sup> for  $\alpha$ -1 and  $\alpha$ -2, respectively. For 1, the *exodentate* phases were again found to be very similar (188.92 and 188.34 kJ mol<sup>-1</sup> for  $\beta$ -1 and  $\gamma$ -1, respectively) with the difference in CE between  $\beta$ -2 and the hypothetical  $\gamma$ -2 phases being slightly larger (188.92 and 186.41 kJ mol<sup>-1</sup>, respectively). These data corroborate the conclusions drawn above.

In  $\gamma$ -1 the charge on the Pd(II) center is calculated as being 0.72 e, whereas in  $\gamma$ -2 the charge on the Pt(II) center is predicted to be only 0.36 e (Table A3 of Supporting Information); the charge on the macrocyclic O donor is found to be the same in both phases (0.49 e). A stronger M...O interaction would be expected in  $\gamma$ -1 than in  $\gamma$ -2, since a hard O donor would experience greater electrostatic attraction to the more highly charged Pd(II) center. Given that the metal centers are otherwise shielded from their surroundings by the remaining atoms in the molecule, and the comparatively small differences in the charges of these other atoms between the phases, the chain-forming M...O interaction constitutes the principal distinction between the intermolecular interactions in the two phases. The CEs indicate a slightly weaker set of intermolecular interactions in  $\gamma$ -2 compared with  $\gamma$ -1 (186.41 and 188.34 kJ mol<sup>-1</sup>, respectively). These comparisons lend weight to the inference that the chain-forming interaction between the metal center and macrocyclic O donor of the  $\gamma$

**Table 5.** Selected Interatomic Distances (Å) for  $\beta$ -1,  $\beta$ -2, and  $\beta$ -1-epitaxy<sup>a</sup>

phase	M...M	M...O	M-S4	M-S7	M-Cl1	M-Cl2
$\beta$ -1	3.4946(7)	3.404(3)	2.2699(11)	2.2601(12)	2.3124(11)	2.3214(11)
$\beta$ -2	3.5294(2)	3.450(2)	2.2542(7)	2.2494(7)	2.3221(8)	2.3266(8)
$\beta$ -1-epitaxy	3.4937(6)	3.406(3)	2.2729(10)	2.2604(10)	2.3168(11)	2.3265(11)

<sup>a</sup>The values for  $\beta$ -1-epitaxy are generally much closer to those of  $\beta$ -1 than of  $\beta$ -2.

phase would be weaker for **2** than it is for **1**. Given the likely role of the M $\cdots$ O interaction in the formation of the  $\gamma$  phase, its relative weakness in **2** provides further rationalization for the absence of the  $\gamma$ -**2** phase.

## CONCLUSIONS

In two new phases of [PdCl<sub>2</sub>([9]aneS<sub>2</sub>O)] (**1**), designated  $\beta$ -**1** and  $\gamma$ -**1** in order of their discovery, the [9]aneS<sub>2</sub>O macrocycle adopts *exodentate* conformations, in contrast to the *endodentate* conformation found in the previously reported  $\alpha$ -**1** polymorph. We also report two phases of the previously unreported complex [PtCl<sub>2</sub>([9]aneS<sub>2</sub>O)] (**2**), designated  $\alpha$ -**2** and  $\beta$ -**2**, which are isomorphous and isostructural with the correspondingly designated phases of **1**. The inability to reproduce the crystallization of  $\beta$ -**1** by standard methods led us to the conclusion that  $\beta$ -**1** is a “disappearing polymorph”, with  $\gamma$ -**1** being the preferred *exodentate* form of **1**. In contrast,  $\beta$ -**2** is the only phase of **2** obtained in this investigation which exhibits an *exodentate* conformation for the macrocycle. No polymorph of **2** corresponding to  $\gamma$ -**1** has been isolated thus far despite attempts to seed its growth using a crystal of the latter phase.

A crystal of  $\beta$ -**2** was successfully used to seed the epitaxial growth of the disappearing polymorph  $\beta$ -**1**, and the resulting crystals were shown by MALDI mass spectrometry and single crystal X-ray diffraction to be free from any significant content of **2**.

DFT analysis reveals the order of phase stability to be  $\alpha > \beta \approx \gamma$  for **1** and  $\alpha > \beta > \gamma$  for **2** (where the  $\gamma$ -**2** phase is hypothetical and based on the structure of  $\gamma$ -**1**). There is a greater difference between the energies for polymorphs of **2** than for polymorphs of **1**. However, from these results alone, the polymorphic behavior observed for **1** cannot be fully understood.  $\beta$ -**1** exhibits a partial  $\beta \rightarrow \alpha$  phase transformation brought about by the mechanical pressure of cutting the crystal, whereas no such phase transition on cutting is observed for  $\beta$ -**2**. This suggests that the  $\beta$  phase lies in a potential energy well close to that of the stable *endodentate*  $\alpha$  phase and that the energy barrier between them is particularly low in the case of **1**. The  $\beta$ -**1** form is, therefore, not recoverable by conventional recrystallization as the  $\beta \rightarrow \alpha$  transformation is facile in the early stages of crystal growth. In  $\gamma$ -**1**, not only do intermolecular Pd $\cdots$ O and C–H $\cdots$ Cl interactions give rise to chains of molecules, they may also stabilize the *exodentate* conformer of the macrocycle during crystal growth; these interactions appear weaker in  $\gamma$ -**2** and so would not stabilize growth of this phase to the same extent.

## ASSOCIATED CONTENT

### Supporting Information

Crystal data and crystallographic experimental tables, the results of geometry optimization calculations, selected partial atomic charges derived from the Mulliken population analysis and details of intramolecular and intermolecular geometry. Crystallographic Information Files (CIFs) are also available. This material is available free of charge via the Internet at <http://pubs.acs.org>.

## AUTHOR INFORMATION

### Corresponding Authors

\*E-mail: A.J.Blake@Nottingham.ac.uk.

\*E-mail: M.Schroder@Nottingham.ac.uk.

## Notes

The authors declare no competing financial interest.

## ACKNOWLEDGMENTS

The authors acknowledge funding support from the UK EPSRC and from The University of Nottingham. M.S. gratefully acknowledges receipt of an ERC Advanced Grant (number 226593). We thank Mr. Graham Coxhill and Dr. William Lewis for their experimental assistance.

## REFERENCES

- (1) Stahly, G. P. *Cryst. Growth Des.* **2007**, *7*, 1007–1026.
- (2) Cruz-Cabeza, A. J.; Bernstein, J. *Chem. Rev.* **2014**, *114*, 2170–2191.
- (3) Allen, F. H. *Acta Crystallogr., Sect. B* **2002**, *58*, 380–388.
- (4) Braga, D.; Grepioni, F.; Desiraju, G. R. *Chem. Rev.* **1998**, *98*, 1375–1405.
- (5) Braga, D.; Grepioni, F. *Chem. Soc. Rev.* **2000**, *29*, 229–238.
- (6) McCrone, W. C. *Physics and Chemistry of the Organic Solid State*; Fox, D., Labes, M. M., Weissberger, A., Eds; Interscience: New York, 1965; Vol. 2, p 727.
- (7) Blagden, N.; de Matas, M.; Gavan, P. T.; York, P. *Adv. Drug Delivery. Rev.* **2007**, *59*, 617–630.
- (8) Llinas, A.; Goodman, J. M. *Drug Discovery Today* **2008**, *13*, 198–210.
- (9) Dunitz, J. D.; Bernstein, J. *Acc. Chem. Res.* **1995**, *28*, 193–200.
- (10) Bombicz, P.; Czugler, M.; Tellgren, R.; Kálmán, A. *Angew. Chem., Int. Ed.* **2003**, *42*, 1957–1960.
- (11) Czugler, M.; Kálmán, A.; Kovács, J.; Pintér, I. *Acta Crystallogr., Sect. B* **1981**, *37*, 172–177.
- (12) Bauer, J.; Spanton, S.; Henry, R.; Quick, J.; Dziki, W.; Porter, W.; Morris, J. *Pharm. Res.* **2001**, *18*, 859–866.
- (13) Wong, M. H.; Keller, S.; Nidhi; Dasgupta, S.; Denninghoff, D. J.; Kolluri, S.; Brown, D. F.; Lu, J.; Fichtenbaum, N. A.; Ahmadi, E.; Singiseti, U.; Chini, A.; Rajan, S.; DenBaars, S. P.; Speck, J. S.; Mishra, U. K. *Semicond. Sci. Technol.* **2013**, *28*, 074009.
- (14) Liu, B.; Fischer, R. A. *Sci. China Chem.* **2011**, *54*, 1851–1866.
- (15) Braga, D.; Cojazzi, G.; Maini, L.; Polito, M.; Grepioni, F. *Chem. Commun.* **1999**, 1949–1950.
- (16) Mitchell, C. A.; Yu, L.; Ward, M. D. *J. Am. Chem. Soc.* **2001**, *123*, 10830–10839.
- (17) Munroe, Á.; Croker, D.; Hodnett, B. K.; Seaton, C. C. *CrystEngComm* **2011**, *13*, 5903–5907.
- (18) Stoica, C.; Tinnemans, P.; Meekes, H.; Vlieg, E. *Cryst. Growth Des.* **2005**, *5*, 975–981.
- (19) Lang, M.; Grzesiak, A. L.; Matzger, A. J. *J. Am. Chem. Soc.* **2002**, *124*, 14834–14835.
- (20) Price, C. P.; Grzesiak, A. L.; Matzger, A. J. *J. Am. Chem. Soc.* **2005**, *127*, 5512–5517.
- (21) Shaw, J. L.; Wolowska, J.; Collison, D.; Howard, J. A. K.; McInnes, E. J. L.; McMaster, J.; Blake, A. J.; Schröder, M. *J. Am. Chem. Soc.* **2006**, *128*, 13827–13839.
- (22) Stephen, E.; Huang, D.; Shaw, J. L.; Blake, A. J.; Collison, D.; Davies, E. S.; Edge, R.; Howard, J. A. K.; McInnes, E. J. L.; Wilson, C.; Wolowska, J.; McMaster, J.; Schröder, M. *Chem., Eur. J.* **2011**, *17*, 10246–10258.
- (23) Allan, D. R.; Bailey, D.; Bird, N.; Blake, A. J.; Champness, N. R.; Huang, D.; Keane, C. P.; McMaster, J.; Prior, T. J.; Tidey, J. P.; Schröder, M. *Acta Crystallogr., Sect. B* **2014**, *70*, 469–486.
- (24) *CrysAlis<sup>Pro</sup>*; Agilent Technologies Ltd, Yarnton, England, UK, specific versions shown in Supporting Information.
- (25) Sheldrick, G. M. *Acta Crystallogr., Sect. A* **2008**, *64*, 112–122.
- (26) Dolomanov, O. V.; Bourhis, L. J.; Gildea, R. J.; Howard, J. A. K.; Puschmann, H. *J. Appl. Crystallogr.* **2009**, *42*, 339–341.
- (27) Perdew, J. P.; Burke, K.; Ernzerhof, M. *Phys. Rev. Lett.* **1996**, *77*, 3865–3868.
- (28) Clark, S. J.; Segall, M. D.; Pickard, C. J.; Hasnip, P. J.; Probert, M. I. J.; Refson, K.; Payne, M. C. *Z. Kristallogr.* **2005**, *220*, 567–570.

- (29) Monkhorst, H. J.; Pack, J. D. *Phys. Rev. B* **1976**, *13*, 5188–5192.
- (30) Grimme, S. J. *Comput. Chem.* **2006**, *27*, 1787–1799.
- (31) Tkatchenko, A.; Scheffler, M. *Phys. Rev. Lett.* **2009**, *102*, 073005.
- (32) Lucas, C. R.; Liang, W.; Miller, D. O.; Bridson, J. N. *Inorg. Chem.* **1997**, *36*, 4508–4513.
- (33) Bondi, A. J. *J. Phys. Chem.* **1964**, *68*, 441–451.
- (34) Bernstein, J.; Davis, R. E.; Shimoni, R.; Chang, N.-L. *Angew. Chem., Int. Ed. Engl.* **1995**, *34*, 1555–1573.
- (35) Macrae, C. F.; Bruno, I. J.; Chisholm, J. A.; Edgington, P. R.; McCabe, P.; Pidcock, E.; Rodriguez-Monge, L.; Taylor, R.; van de Streek, J.; Wood, P. A. *J. Appl. Crystallogr.* **2008**, *41*, 466–470.
- (36) Bernstein, J. *Polymorphism in Molecular Crystals*; International Union of Crystallography/Oxford University Press: Oxford, 2002; pp 40–41.